Determining Multiscale Image Feature Angles from Complex Wavelet Phases

Ryan Anderson, Nick Kingsbury, Julien Fauqueur*

Signal Processing Group, Dept. of Engineering, University of Cambridge, UK

Abstract. In this paper, we introduce a new multiscale representation for 2-D images named the *Inter-Coefficient Product (ICP)*. The ICP is a decimated pyramid of complex values based on the Dual-Tree Complex Wavelet Transform (DT-CWT). The complex phases of its coefficients correspond to the angles of dominant directional features in their support regions. As a sparse representation of this information, the ICP is relatively simple to calculate and is a computationally efficient representation for subsequent analysis in computer vision activities or large data set analysis. Examples of ICP decomposition show its ability to provide an intuitive representation of multiscale features (such as edges and ridges). Its potential uses are then discussed.

1 Introduction

Wavelets, once used primarily for compression, have found new uses for image content analysis. The ability of the wavelet transform to isolate image energy concisely into spatial, directional, and scalar components have allowed it to characterize the multiscale profile of non-stationary signals, including 2-D images, very effectively. In particular, complex wavelets have shown a strong ability to consistently represent object structures in 2-D images for object recognition and computer vision activities.

In this paper, we explore methods of building upon the phase information of complex wavelets to yield intuitive image representations. To date, complex wavelet *magnitudes* have typically been used in place of real wavelets to improve the consistency of segmentation, denoising, etc. However, phase information, which indicates the offset of directional features within the support region of a wavelet coefficient, has found less application to date in analysis and coding applications (although stereo matching and motion estimation are two examples of its use). Recently, in [3], Romberg et al. have described a probabilistic model, the Geometric Hidden Markov Tree (GHMT), which uses phase as well as magnitude information to infer the angle and offset of contour segments in the vicinity of a complex wavelet coefficient. In this paper, we introduce a faster method to calculate the angle of directional energy in the vicinity of a coefficient. This method, which we have named the *Inter-Coefficient Product (ICP)*, may find use in large-scale image analysis or real-time computer vision, where computational complexity must be minimized. We introduce the ICP as a complement to another phase-based transform, the Interlevel Product (ILP) [1]. Upon describing the background of complex wavelets (section 2), we will develop the ICP transform in section 3 and show example ICP decompositions in section 4. We conclude in section 5 with a discussion of potential uses of the ICP and its relationship to the DT-CWT and the ILP.

* This work has been carried out with the support of the UK Data & Information Fusion Defence Technology Centre.

2 The Dual-Tree Complex Wavelet Transform

Standard real wavelets, such as the Haar and Daubechies wavelets, suffer from *shift dependence*. Shift dependence implies that the decomposition of image energy between levels of a multiscalar decomposition can vary significantly, if the original image is shifted prior to decomposition. This variation limits the effectiveness of the real wavelet transform to consistently represent an image object at multiple scales.

Complex wavelets, including the linearly-separable Dual-Tree Complex Wavelet [2] have been created to address the problems of shift dependence. A complex wavelet is a set of two real wavelets with a 90° phase difference. For 2-D image analysis, the DT-CWT produces $d = 1 \ldots 6$ directional subbands at approximately $\frac{\pi}{10}$, $\frac{\pi}{4}$, $\frac{2\pi}{5}$, $\frac{3\pi}{5}$, $\frac{3\pi}{4}$, and $\frac{9\pi}{10}$ (for convenience, these subbands are often labelled with equally-spaced angles of 15°, 45°, 75°, 105°, 135°, and 165° respectively). The impulse responses in each of these subbands are shown in figure 1. We note that the magnitude responses of each these subbands can be used to infer feature orientations. However, the lack of precision in these methods is the primary motivation for us to seek a superior representations through the use of complex phase information.

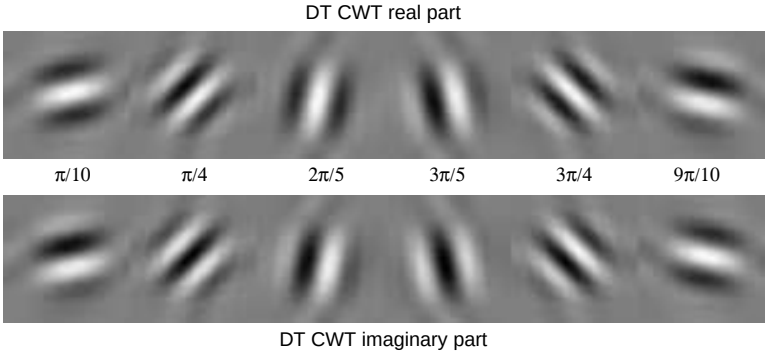

Fig. 1. The real and imaginary impulse responses of the DT-CWT for each of the six subbands.

Figure 2 shows both the phase (fig. 2a) and magnitude (fig. 2b) responses of a DT-CWT coefficient to a shifting step response in 1-D. In particular, we observe that this phase response is consistently *linear* with respect to the feature offset, in the vicinity of the wavelet coefficient. If we define D_W as the distance between adjacent coefficients, as indicated by the vertical lines in figure 2a, then we have experimentally determined the relationship between coefficient phase and feature offset to be $-4.49/D_W$ radians per unit length. With this ratio, we can convert DT-CWT phase to a spatial offset of an edge or impulse, or vice-versa.

In the 2-D case, the phase and magnitude relationships described above apply to edges and ridges oriented in the direction of the subband. The ratios for 2-D subbands differ from the 1-D example; for subbands 1, 3, 4, and 6, the ratio is $-4.49/\left(D_W \cos\frac{\pi}{10}\right)$ or $-4.72/D_W$ radians per unit length. For subbands 2 and 5, the ratio is $-4.49/\left(D_W \cos\frac{\pi}{4}\right)$ or $-6.35/D_W$ radians per unit length. for

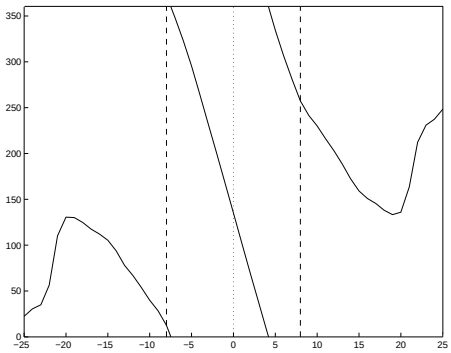

a) The complex phase of a decimated level 3 DT-CWT coefficient (located at the central dotted line), in the presence of a step edge at all possible offsets (the x axis). Note that when an edge or ridge occurs anywhere between the coefficient and its immediate neighbours (shown as the vertical dashed lines), the phase response is linear. This linearity will be used to infer the offset of the edge, relative to the coefficient location, at this scale.

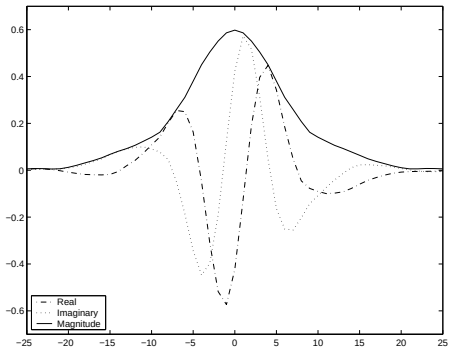

b) The magnitude response of the same DT-CWT coefficient under the same conditions. The overall magnitude is calculated from real and imaginary components, as shown.

Fig. 2. Illustration in the 1-D case of the behaviour of the phase and magnitude of a DT-CWT coefficient (level 3, in this case) in the presence of a step edge, at the indicated x coordinate, relative to the coefficient.

these 2-D cases, the *subband offset* of a feature is defined in the direction normal to the subband, as shown in figure 3.

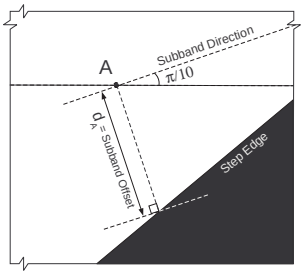

Fig. 3. Definition of the subband offset d_A in the 2-D case between a coefficient location A and a step edge.

3 The Inter-Coefficient Product

In this section, we introduce the Inter-Coefficient Product (ICP). We begin in sections 3.1 and 3.2 by showing how the orientation of a 2-D feature (such as an edge or ridge) can be determined from the phase difference of two adjacent DT-CWT coefficients. This derivation leads us naturally to the definition of the ICP in section 3.3.

3.1 Determination of feature orientation from neighbour coefficients

Consider Figure 4, which shows a feature (a step edge, in this case) that spans the support regions of two horizontally adjacent DT-CWT coefficients at locations $A=(x,y)$ and $B=(x+1,y)$, at some arbitrary level. This figure illustrates the trigonometric relationship between the angle of the feature and its subband offsets with respect to these coefficients.

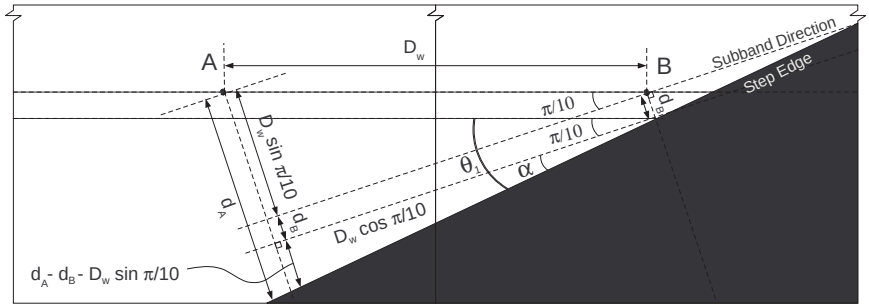

Fig. 4. Trigonometric relationship between the angle $\theta_1 = \alpha + \frac{\pi}{10}$ of a feature (step edge, in this case) and its subband offsets d_A and d_B to two horizontally adjacent $\frac{\pi}{10}$ subband DT-CWT coefficients located at $A=(x,y)$ and $B=(x+1,y)$.

As this step edge is closest to the $d=1$, $\frac{\pi}{10}$ subband, the DT-CWT coefficients $W_l(x,y,1)$ and $W_l(x+1,y,1)$ will correspondingly have large magnitudes in this subband only. From figure 4, we can see that the angle of the feature, θ_1, can be calculated as

$$\theta_1 = \frac{\pi}{10} + \alpha = \frac{\pi}{10} + \tan^{-1}\frac{d_A - d_B - D_w \sin\frac{\pi}{10}}{D_w \cos\frac{\pi}{10}} \tag{1}$$

where d_A and d_B are the subband offsets of the edge to the two coefficients as defined in figure 3, using subband 1. These two offset lengths are equal to $\frac{D_W}{4.72}\angle W_l(x,y,1)$ and $\frac{D_W}{4.72}\angle W_l(x+1,y,1)$ respectively[1], according to our phase/offset relationships described at the end of section 2. Thus, we

[1] We denote the phase argument of a complex number c as $\angle c = arg(c)$.

can rewrite Equation (1) as

$$\theta_1 = \frac{\pi}{10} + \tan^{-1} \frac{\frac{D_W}{4.72}\angle W_l(x,y,1) - \frac{D_W}{4.72}\angle W_l(x+1,y,1) - D_w \sin\frac{\pi}{10}}{D_w \cos\frac{\pi}{10}}$$
$$= \frac{\pi}{10} + \tan^{-1}\left[\frac{\angle W_l(x,y,1) - \angle W_l(x+1,y,1)}{4.72\cos\frac{\pi}{10}} - \tan\frac{\pi}{10}\right] \quad (2)$$

We note that for $-\frac{\pi}{5} < \alpha < \frac{\pi}{5}$, which is the approximate range of feature angles that will contribute to an individual subband, we can assume that $\alpha \approx \tan\alpha$. Applying this approximation twice to Equation (2), we can simplify this expression to

$$\theta_1 = \frac{\pi}{10} + \frac{\angle W_l(x,y,1) - \angle W_l(x+1,y,1)}{4.72\cos\frac{\pi}{10}} - \frac{\pi}{10} \quad (3)$$
$$\Rightarrow \theta_1 = \frac{1}{4.49}[\angle W_l(x,y,1) - \angle W_l(x+1,y,1)] \quad (4)$$

Thus, for subband 1, we merely divide the phase difference between two horizontally adjacent DT-CWT coefficients by 4.49 to obtain the angle of the dominant feature in their vicinity.

3.2 Feature orientation calculations for all subbands

In the previous section example, we considered the $\frac{\pi}{10}$ subband ($d = 1$) given the orientation of our particular example of step edge. In the general case, to detect a feature at any orientation, the same type of calculation is achieved for all six subbands based on phase difference between appropriate neighbour DT-CWT coefficients: we compare horizontal neighbours for the $\frac{\pi}{10}$ and $\frac{9\pi}{10}$ subbands ($d = 1, 6$), vertical neighbours for the $\frac{2\pi}{5}$ and $\frac{3\pi}{5}$ subbands ($d = 3, 4$), and diagonal neighbours for the $\frac{\pi}{4}$ and $\frac{3\pi}{4}$ subbands ($d = 2, 5$). Thus six orientation angles are calculated $\theta_1, ..., \theta_6$, one for each subband. We have already determined θ_1 (see Equation (4)).

By symmetry, the geometric relationship in the $\frac{\pi}{10}$ subband $d = 1$ can be equally applied to subbands $d = 3, 4$, and 6, where feature angles in subbands 3 and 4 are measured relative to the vertical axis. For these two subbands, therefore, we would therefore modify equation (4) to add $\frac{\pi}{2}$ to the angle. However, in the $\frac{\pi}{4}$, $\frac{3\pi}{4}$ subbands 2 and 5, the W_l values possess a different relationship with the angles of dominant features with two diagonally adjacent coefficients. Using subband 2, the angle of the feature is related to coefficient offsets by the following simpler equation:

$$\theta_2 = \frac{\pi}{4} + \tan^{-1}\frac{d_A - d_B}{\sqrt{2}D_w} \quad (5)$$

Performing the same substitutions, assumptions, and simplifications as with our previous example, we establish the linear relationship between θ_2 and the W_l coefficient phases to be

$$\theta_2 = \frac{\pi}{4} + \frac{1}{8.98}[\angle W_l(x,y+1,2) - \angle W_l(x+1,y,2)] \quad (6)$$

As with the previous example, this relationship is identical for subband 5, except that $\frac{3\pi}{4}$ would be added to the phase of θ_5 in the operation above.

3.3 Definition of ICP

In the previous section, we established the linear relationship formulae between a feature orientation and the difference of phase between adjacent DT-CWT complex coefficients. We calculate these phase differences by means of conjugate products of the adjacent pairs of DT-CWT coefficients as detailed in the previous section. The complex products are a natural way to represent the feature orientation (through the complex phase) and also the feature strength (through the complex magnitude). Thus, if we consider $W_l(x, y, d)$ to be the complex DT-CWT coefficient at spatial location x, y (numbered from the top left corner), subband d, and level l, then we introduce the constant-phase complex values $W_{l\Delta}$:

$$\begin{aligned}
W_{l\Delta}(x,y,1) &= W_l(x,y,1) &&\times W_l(x+1,y,1)^* \\
W_{l\Delta}(x,y,2) &= W_l(x,y+1,2) &&\times W_l(x+1,y,2)^* \\
W_{l\Delta}(x,y,3) &= W_l(x,y,3) &&\times W_l(x,y+1,3)^* \\
W_{l\Delta}(x,y,4) &= W_l(x,y,4)^* &&\times W_l(x,y+1,4) \\
W_{l\Delta}(x,y,5) &= W_l(x,y,5)^* &&\times W_l(x+1,y+1,5) \\
W_{l\Delta}(x,y,6) &= W_l(x,y,6)^* &&\times W_l(x+1,y,6)
\end{aligned} \tag{7}$$

From this definition, the feature orientation θ_d calculated for each subband d in the previous section, can be expressed with respect to $\angle W_{l\Delta}(x, y, d)$. For instance, from equation (4), $\theta_1 = \frac{1}{4.49}\angle W_{l\Delta}(x, y, 1)$.

The magnitudes of $W_{l\Delta}$ are the product of the magnitudes of the two adjacent DT-CWT coefficients, and the phases of $W_{l\Delta}$ are their shift-invariant phase differences. Note that we can divide the magnitudes of $W_{l\Delta}$ by $\sqrt{|\ W_{l\Delta}\ |}$ to mitigate the non-linear product effect of this operation.

Using the conjugate products $W_{l\Delta}$ and the expressions for feature orientations θ_d, we now define the Inter-Coefficient Product.

Definition 1 (Inter-Coefficient Product) *Given a DT-CWT decomposition of an image with coefficients $W_l(x, y, d)$ for levels l and subbands $d = 1, ..., 6$, we define the Inter-Coefficient Product (ICP) for each subband d, level l and decimated location (x, y) as the following set of complex coefficients $\{\psi_l(x, y, d), d = 1, ..., 6\}$:*

$$\begin{aligned}
\psi_l(x,y,1) &= \sqrt{|\ W_{l\Delta}(x,y,1)\ |} \times e^{i(\frac{1}{4.49}\angle W_{l\Delta}(x,y,1))} \\
\psi_l(x,y,2) &= \sqrt{|\ W_{l\Delta}(x,y,2)\ |} \times e^{i(\frac{\pi}{4}+\frac{1}{8.98}\angle W_{l\Delta}(x,y,2))} \\
\psi_l(x,y,3) &= \sqrt{|\ W_{l\Delta}(x,y,3)\ |} \times e^{i(\frac{\pi}{2}+\frac{1}{4.49}\angle W_{l\Delta}(x,y,3))} \\
\psi_l(x,y,4) &= \sqrt{|\ W_{l\Delta}(x,y,4)\ |} \times e^{i(\frac{\pi}{2}+\frac{1}{4.49}\angle W_{l\Delta}(x,y,4))} \\
\psi_l(x,y,5) &= \sqrt{|\ W_{l\Delta}(x,y,5)\ |} \times e^{i(\frac{3\pi}{4}+\frac{1}{8.98}\angle W_{l\Delta}(x,y,5))} \\
\psi_l(x,y,6) &= \sqrt{|\ W_{l\Delta}(x,y,6)\ |} \times e^{i(\frac{1}{4.49}\angle W_{l\Delta}(x,y,6))}
\end{aligned}$$

where $i = \sqrt{-1}$.

We will consider the contribution of a feature to the subband which is the closest to its orientation, since it is where the DT-CWT coefficient response is linear and the strongest. The coefficient magnitudes automatically reveal the dominant orientation of the feature across subbands.

At each location (x, y) and each level l, the orientation of a potential feature (such as an edge or a ridge) in the vicinity of (x, y) will be given by the phase of an ICP coefficient. The magnitude of the ICP coefficient will reflect the strength of this feature.

4 Results and Interpretation

Figure 5 shows an ICP decomposition for the "Lenna" image, for level $l = 3$, $\frac{9\pi}{10}$ subband in figure 5a, and level $l = 4$ (coarser), $\frac{\pi}{4}$ subband in figure 5b. When overlayed upon the original image, we can see the ability of the ICP to follow coarse and fine image contours.

If we shift the original image half the current subband coefficient spacing prior to ICP transform, we apply the worst possible offset in multiscale misalignment (described in [1]) that may occur if one was to compare two separate instances of an image object. Figure 6 shows this offset; note that, relative to figure 5b, the coefficients make small, predictable changes in direction and magnitude to reflect changing support regions, but dominant edge features in the image keep the coarse-level representation relatively invariant to multiscale misalignment, which shows the shift independence of ICP.

Note also that the ICP is a reversible transform; with all the ICP coefficients and the last row and column of DT-CWT coefficients, one can divide out all of the original DT-CWT coefficients one row/column at a time (and thence reconstruct the original image with a reverse DT-CWT transform). However, as the ICP itself acts in the manner of a differential operator, modifications to the ICP coefficients can propagate throughout the image, far beyond the support range of the original coefficient.

(a) **(b)**

Fig. 5. ICP Coefficients for "Lenna" picture, at a) Level 3, Subband 6; and b) Level 4, Subband 2. Note the ability of the ICP to follow, for example, the fine edge of the top of the hat in a), and the coarse-scale $\frac{\pi}{4}$ rim of the hat on the left in b).

Fig. 6. ICP shift independence: the input image of figure 5b has been shifted by half a sample in each direction prior to ICP transform. Although this shift corresponds to the worst alignment case, we observe minor changes in the ICP coefficients.

5 Conclusions

The ICP transform extracts phase information from the DT-CWT transform into an intuitive, sparse format that reveals the orientation of directional features with finer precision than with the sole use of magnitudes of real or complex wavelets coefficients. The entire process from pixel domain to ICP domain is efficient to implement: the DT-CWT is linearly separable into row and column operations, and the subsequent ICP operation performs simple operations on decimated coefficients. Thus, we believe ICP coefficients to be appropriate for multiscale image processing activities such as contour tracking, registration, and rotation- and scale-invariant object recognition, in large images or real-time systems where computational complexity is a strong factor in system design.

In particular, we note that the ICP and the ILP [1] transforms complement one another very eloquently in the description of multiscale features. The ICP is highly informative as to small rotations and relatively insensitive to feature structure. By contrast, the ILP is indicative of the nature of the feature itself and is insensitive to small rotations. Between these two pyramidal image representation transforms, we can build a highly informative hybrid representation of image objects that can be detected at various scales and rotations. Our future research will pursue such models with these coefficients.

References

1. R. Anderson, N. Kingsbury, and J. Fauqueur. Coarse level object recognition using interlevel products of complex wavelets. In *International Conference on Image Processing (ICIP)*, September 2005.
2. N.G. Kingsbury. Complex wavelets for shift invariant analysis and filtering of signals. *Journal of Applied and Computational Harmonic Analysis*, (3):234–253, 2001.
3. J. Romberg, M. Wakin, H. Choi, and R. Baraniuk. A Geometric Hidden Markov Tree Wavelet Model. In *SPIE Wavelets X*, San Diego, CA, August 2003.